

A Virtual Wind Tunnel for Numerical Simulation of Flow-Induced Vibrations

Kyoji Kamemoto

Yokohama National University, 79-5 Tokiwadai, Hodogaya-ku, Yokohama, 240-8501 Japan

Akira Ojima

College Master Hands Inc., 2-1-31 Midorigaoka, Zama, 228-0021 Japan

Akihiro Nakamura

Yokohama National University, 79-5 Tokiwadai, Hodogaya-ku, Yokohama, 240-8501 Japan

ABSTRACT

A virtual wind tunnel (VWT) based on a vortex method has been developed to analyze complex, unsteady and vortical flows in relation to problems in a wide range of industries. In order to confirm applicability of the VWT for the problems of flow induced vibrations, it has applied to the simulation of flows around a stationary circular cylinder and an elastic one, for flow conditions and structural configurations reported in the past literature. The calculated results are presented and applicability of the VWT is discussed making reference to the past experiments

1. INTRODUCTION

The consideration of vortex-induced vibrations (VIV) of slender and circular-cylindrical bodies is very important in the design of various structures in industries. So far, despite the relatively fundamental phenomena of the VIV, only a comparatively small amount of knowledge is accumulated about the nature of the fluid-structure interaction

For investigation of response of structure in vortex-induced vibration, various experimental works have been performed by employing the method of free-vibration testing (Feng 1968, King 1977). And numerical investigation is an alternative way to solve the fully coupled problem of VIV of bluff bodies. Many researchers have worked to apply the techniques of computational fluid dynamic (CFD) to solve the problem of VIV. Meneghini and Bearman (1995) and Zhou (1999) used the vortex-in-cell (VIC) method to solve the problem of 2D incompressible flow past an oscillating circular cylinder or an elastic one. Evangelinos et al. (2000) used direct numerical simulation (DNS) based on spectral elements to simulate the 3D flow past rigid and flexible cylinders. Willden and Graham (2001) used a quasi-3D extension of the strip theory to simulate the low Reynolds number VIV of a long flexible circular cylinder with a low mass ratio and zero damping. It is known, however, that still there exist technical

difficulties associated with numerical analysis of flows around moving boundaries, although various types of meshing as overlapping, sliding grids and Cartesian grids have been examined.

On the other hand, the vortex methods have been developed and applied for analysis of complex, unsteady and vortical flows in relation to problems in a wide range of industry, because they consist of simple algorithm based on physics of flow. Nowadays, applicability of the vortex element methods has been developed and improved dramatically, and it has become encouragingly clear that the vortex methods have so much interesting features that they provide easy-to-handle and completely grid-free Lagrangian calculation of unsteady and vortical flows without use of any RANS type turbulence models. Details can be found in Leonard (1980), Sarpkaya (1989) and Kamemoto (1995).

As well as many finite difference methods, it is a crucial point in vortex methods that the number of vortex elements should be increased when higher resolution of turbulence structures is required, and then the computational time increases rapidly. In order to reduce the operation count of evaluating the velocity at each particle through a Biot-Savart law, fast N-body solvers, by which the operation count is reduced from $O(N^2)$ to $O(N \log N)$, have been proposed by Greengard et al. (1987). On the other hand, in order to reduce the computational load in calculation of turbulence structures, Fukuda and Kamemoto (2005) proposed an effective redistribution model of vortex elements with consideration of convective motion and viscous diffusion in a three dimensional core-spreading model.

In the present study, in order to examine the applicability of the virtual wind tunnel based on the vortex method developed to extend as a tool for a grid-free Lagrangian large eddy simulation by the present authors to fluid dynamics in VIV problem, numerical simulation of three dimensional, complex and unsteady flows around an elastic circular cylinder were performed. From the numerical

analyses, vortical flow characteristics around the elastic circular cylinder have been investigated and numerical results were compared with experimental ones.

2. NUMERICAL SCHEMES

2.1 Vortex methods

The governing equations of viscous and incompressible flow are described by the vorticity transport equation and the pressure Poisson equation which can be derived by taking the rotation and the divergence of Navier-Stokes equations, respectively.

$$\frac{\partial \bar{\omega}}{\partial t} + (\bar{u} \cdot \text{grad}) \bar{\omega} = (\bar{\omega} \cdot \text{grad}) \bar{u} + \nu \nabla^2 \bar{\omega} \quad (1)$$

$$\nabla^2 p = -\rho \text{div}(\bar{u} \cdot \text{grad} \bar{u}) \quad (2)$$

Where \bar{u} is a velocity vector and a vorticity $\bar{\omega}$ is defined as follows:

$$\bar{\omega} = \text{rot} \bar{u} \quad (3)$$

As explained by Wu and Thompson (1973), the Biot-Savart law can be derived from the definition equation of vorticity as follows:

$$\begin{aligned} \bar{u} = & \int_V (\bar{\omega}_0 \times \nabla_0 G) dv \\ & + \int_S \{ (\bar{n}_0 \cdot \bar{u}_0) \cdot \nabla_0 G - (\bar{n}_0 \times \bar{u}_0) \times \nabla_0 G \} ds \end{aligned} \quad (4)$$

Here, subscript "0" denotes variable, differentiation, and integration at a location \bar{r}_0 , and \bar{n}_0 denotes the normal unit vector at a point on a boundary surface S . And G is the fundamental solution of the scalar Laplace equation with the delta function $\delta(\bar{r} - \bar{r}_0)$ in the right hand side, which is written for a three-dimensional field as $G = 1/4\pi|\bar{r} - \bar{r}_0|$.

In equation (4), the inner product $\bar{n}_0 \cdot \bar{u}_0$ and the outer product $\bar{n}_0 \times \bar{u}_0$ stand for normal velocity component and tangential velocity vector on the boundary surface. They correspond to the source distribution on the surface and the vortex distribution that has the rotating axis in parallel to the surface. In this study, a boundary surface is represented by the panel method. The source and vortex corresponding to the second and third terms of right hand side of equation (4) are distributed on the boundary surface. The strengths of source and vortex are obtained by using the following two conditions; zero normal component of relative velocity to the boundary surface $(\bar{u} - \bar{v}_w) \cdot \bar{n} = 0$ and the relation of the conservation of the vortex strength, respectively. \bar{v}_w is a moving velocity of a boundary. The pressure in the field is obtained from the integration equation formulated by Uhlman (1992), instead of the finite difference

calculation of equation (2) as follows:

$$\begin{aligned} \beta H + \int_S H \frac{\partial G}{\partial n} ds = & - \int_V \nabla G (\bar{u} \times \bar{\omega}) dv \\ & - \int_S G \bar{n} \frac{\partial \bar{u}}{\partial t} ds - \nu \int_S \bar{n} (\nabla G \times \bar{\omega}) ds \end{aligned} \quad (5)$$

Here, $\beta = 1$ in the flow field and $\beta = 1/2$ on the boundary S . G is the fundamental solution. H is the Bernoulli function defined as $H = p/\rho + |\bar{u}|^2/2$.

The value of H on the boundary surface is calculated from equation (5) by using the panel method. After the pressure distribution around the boundary surface is calculated from equation (5), integration of the pressure acting on the body surface yields the force acting on the body.

One of the most important schemes in the vortex methods is how to represent the distribution of vorticity in the proximity of the body surface, taking account of viscous diffusion and convection of vorticity under the non-slip condition on the surface. In the present method, a thin vorticity layer is considered along the solid surface, and discrete vortex elements are introduced into the surrounding flow field considering the diffusion and convection of vorticity from discrete elements of the thin vorticity layer. The details of treatments have been explained in the paper by Ojima and Kamemoto (2000). In this paper, they validated the basic technique of the present method by comparisons with experimental results of the flows past a sphere.

The discrete vortex element is modeled by a vortex blob which has a spherical structure with a radially symmetric vorticity distribution proposed by Winkelmann & Leonard (1988). The motion of the discrete vortex elements is represented by Lagrangian form of a simple differential equation $d\bar{r}/dt = \bar{u}$. Then, trajectory of a discrete vortex element over a time step is approximately computed from the Adams-Bashforth method. On the other hand, the evolution of vorticity is calculated by equation (1) with the three-dimensional core spreading method proposed by Nakanishi & Kamemoto (1992). It should be noted here that in order to keep higher accuracy in expression of a local vorticity distribution, a couple of additional schemes of re-distribution of vortex blobs are introduced in the present advanced vortex method. When the vortex core of a blob becomes larger than a representative scale of the local flow passage, the vortex blob is divided into a couple of smaller blobs. On the other hand, if the rate of three-dimensional elongation becomes large to some extent, the vortex blob is divided into plural blobs to approximate the elongated vorticity distribution much more properly.

2.2 Structural dynamics

The procedure to analyze dynamic behavior of structures is based on a beam element representation

using a consistent mass-matrix formulation (i.e., no mass lumping). The resulting equations of motion for each structure are a set of second-order ordinary differential equations (ODEs) of the following form:

$$[M]\ddot{q} + [C]\dot{q} + [K]q = F \quad (6)$$

Where $[M]$ is the mass matrix, $[C]$ is the damping matrix, $[K]$ is the stiffness matrix, q is the vector displacements, and F is the forcing vector. In the three dimensional analysis, the open source finite-element solver CalculiX developed by Dhondt (1998-2004) was used to obtain the structural solutions for the isolated cylinder. The cylinder was assumed to be solid in this study.

Fluid-structure coupling

Within a physical time step, the structural motion and the flow field are unknown and are solved iteratively between the fluid and structural systems in a fully couple manner. The following is the procedure:

- (1) The variables at new time step $n+1$ of the flow and structural equations are initially set to the values of time step n .
- (2) Calculate the pressure and viscous stress exerting on the solid boundary of the body.
- (3) Determine the position of the moving body subject to the fluid forces by solving the structural equations.
- (4) Re-generate the surface mesh and calculate the grid velocity at each node point according to the updated structural position.
- (5) Calculate the flow field by solving the equations of flow motion for the updated mesh and structural position.
- (6) Check the maximum residuals for both solutions of the flow and the structural equations.

If the maximum residuals are greater than the prescribed convergence criteria, go back to step (2) and proceed to the next pseudo time step $m+1$, otherwise the flow field and the movement of the moving body are determined and go back to step (1) to start the next new physical time step $n+1$.

3. APPLICATION TO FLOW-INDUCED VIBRATIONS

3.1 Added-mass effect

In order to confirm the effect of the added mass, the simulations of two-dimensional free oscillating circular cylinder in stationary water was performed.

The cylinder mass ratio $m^* = 4m/\rho_f \pi D^2 L = 7.0$, where m is the mass per unit length of the cylinder length, and ρ_f is the density of fluid. The damping ratio was set as $\zeta = c/(4m\kappa)^{1/2} = 0.0015$. Here, c and κ are the structural damping coefficient and the spring

constant, respectively. Other calculation conditions were set as follows; computational time step $\Delta t = 0.025$ sec and kinematic viscosity of fluid $\nu = 1.1 \times 10^{-6}$ m²/s. As special initial condition, we supposed that the initial load $F_x = -\kappa x_0$ was acting on the cylinder toward x direction. Here, initial displacement was set as $x_0/D = 0.5$.

Figure 2 shows an instantaneous flow pattern represented by vortex elements. Figure 3 shows time history of the displacement of the cylinder. It is confirmed that the amplitude of displacement of the cylinder is decaying with elapsed time. Then, the frequency of x directional displacement of the cylinder was $f_v = 0.4014$ [Hz]. It can be confirmed that the added mass effect was correctly considered in this calculation, because the natural frequency of the cylinder considering the added-mass is $f_n^* = [\kappa/(m+m_A)]^{1/2}/2\pi = 0.3996$ [Hz] as almost the same of calculation result. Here, the added-mass, m_A , is given by $m_A = C_A m'$, where m' is the displaced fluid mass $m' = \rho_f \pi D^2 L/4$ and C_A is the potential added-mass coefficient ($C_A = 1.0$ for a circular cylinder).



Figure 2: Instantaneous flow pattern around oscillating cylinder.

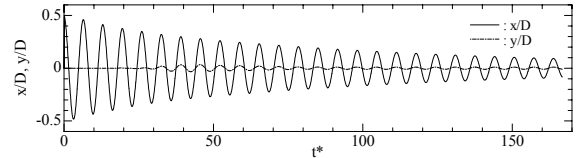


Figure 3: Time histories of cylinder displacement.

3.2 Three-dimensional flexible circular cylinder

In order to confirm the applicability of our code, flow simulation around a stationary circular cylinder and flexible cantilever circular cylinder were performed, and the calculation results were compared with experimental ones.

3.2.1 Stationary circular cylinder

As the calculation model, the circular cylinder model used to the experimental investigation by Jauvtis and Williamson (2004) was employed in this study. Figure 4 shows a diagram of the test equipment. The circular cylinder had an aspect ratio (length/diameter) of $L/D = 10.0$. Reynolds number and time interval were set as $Re = U_0 D/\nu = 2.89 \times 10^3$ and $\Delta t^* = \Delta t U_0/D = 0.1$, respectively. Where U_0 is the free-stream flow speed, and ν is the kinematic viscosity. Here, it should be noted that the upper surface was assumed to be the slip wall

and the mirror condition was imposed in this calculation.

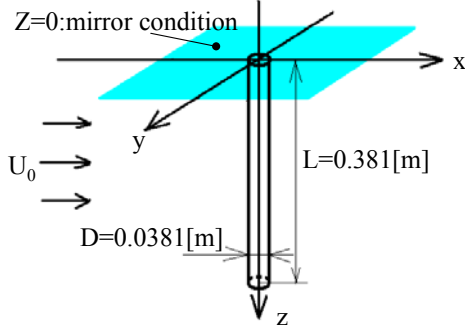


Figure 4: Coordinate system for calculation model.

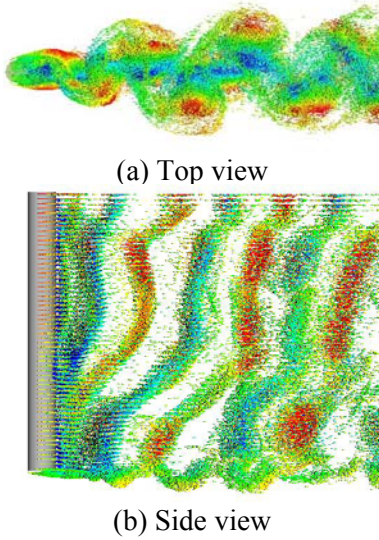


Figure 5: Instantaneous flow pattern around stationary circular cylinder.

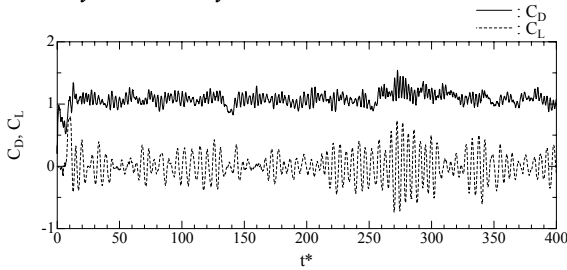


Figure 6: Time variation of fluid force acting on the stationary circular cylinder.

Figure 5 shows a side view and a top view of an instantaneous flow pattern around the stationary circular cylinder at $t^*=tU_0/D=336.0$ expressed by relative velocity vectors at positions of vortex elements. The separated shearlayers shed from the circular cylinder form the structure of Karman vortex street behind the cylinder, and oblique vortex structure, which induced by the free end of the cylinder, were formed behind the cylinder. It is guessed that the present results are the similar phenomena observed from the experimental work by Williamson (1989).

Then, the time variation of each components of fluid force acting on the circular cylinder was shown in figure 6. The time averaged drag coefficient at $150 < t^* < 400$ was $\bar{C}_D = 2\bar{F}_x / \rho U_0^2 DL = 1.07$, and Strouhal number evaluated from the fluctuation of lift coefficient C_L became $St = f_n D / U_0 = 0.20$ in the present calculation. These results are reasonably corresponding compared with past experiment results.

3.2.2 Flexible circular cylinder

The cylinder mass ratio $m^* = 4m / \rho_f \pi D^2 L = 2.6$, where m is the mass per unit length of the cylinder length, and ρ_f is the density of fluid. Here, it should be noted that the damping ratio and gravity were not considered in this calculation. Reynolds numbers and dimensionless dynamic parameters in the present calculations were chosen to match those in the experimental set-up by Jauvtis and Williamson (2004) as shown in Table 2. A reference Reynolds number is $Re = U_0 D / \nu = 2.93 \times 10^3$ at a reduced velocity $V_r = U_0 / f_n D = 5.0$, where U_0 is the average free-stream flow speed and f_n is the free-vibration natural frequency in fluid.

It should be noted that, even with this degree of matching, cylinder-end boundary conditions differ between the experiments and the present calculations, since flexible cantilever circular cylinder with one end free and another end fixed was employed in this calculations.

Table 2: Calculation conditions

Structure	
Density of structure: ρ_s	2.595×10^3 [kg/m ³]
Young's modulus: E	4.265×10^5 [N/m ²]
Pisson's ratio: σ	0.34
Natural frequency: f_n	0.406 [Hz]
Fluid	
Density of fluid: ρ_f	9.982×10^2 [kg/m ³]
Kinematic viscosity: ν	1.004×10^{-6} [m ² /s]

The three-dimensional simulations were carried out for reduced velocities chosen to place near the highest expected amplitude on the upper and lower response branches ($V_r=3.94, 4.93, 5.91, 7.18, 8.53$).

We examined the topology of the vortical wake structure formed behind the flexible cylinder oscillating at the case of $V_r=5.91$. Figure 7 shows the instantaneous flow pattern around the cylinder at $t^*=336.0$ expressed by relative velocity vectors at positions of vortex elements. As shown in Fig. 7, it can be seen vortex dislocations at the case of $V_r=5.91$ are associated with the difference of modes between the bottom and the tip of the cylinder. The present result is very similar to the phenomenon of vortex formation mode which comprises co-rotating vortex pairs for the pivoted circular cylinder by

Flemming and Williamson (2005).

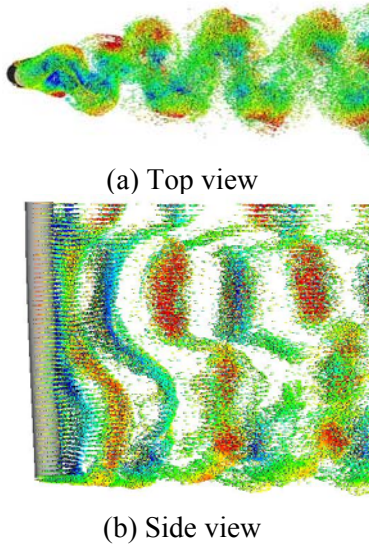


Figure 7: Instantaneous flow pattern around the circular cylinder at reduced velocity $Vr=5.91$.

Figures 8 and 9 are shown in the time variation of each components of fluid force acting on the circular cylinder and the displacement of the tip of cylinder, respectively. It is confirmed that fluid forces acting on the cylinder and the displacement of the cylinder tip are fluctuating according to the variation of vortex wake structure formed behind the cylinder.

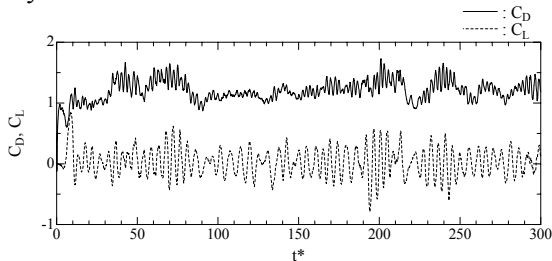


Figure 8: Time histories of fluid force coefficient.

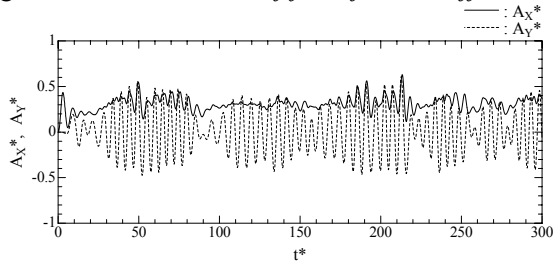


Figure 9: Time histories of displacement of the tip of cylinder.

The amplitude response of the cylinder tip is shown in Fig. 10 and the frequency response of lift force is shown in Fig. 11. Here, the normalized amplitude and frequency are defined as $A_{(x,y)}^* = (x,y)/D$, $f_{(x,y)}^* = f_{(x,y)}/f_n$, respectively. The response amplitudes obtained by present calculations were similar to the experimental results for the case of vibration in two degree freedom of

uniform amplitude to the spanwise direction (Jauvtis and Williamson (2004)). However, these amplitudes obtained by present calculations are somewhat smaller than their experimental results. It is thought likely to be a consequence of the differences in type of the spanwise amplitude distribution.

Transverse frequencies f_y^* , which obtained from sectional lift force acting on the section near the tip ($z/L=0.9$) and mid-span ($z/L=0.5$) of the cylinder, are presented in figure 11, and we have omitted the streamwise frequency f_x^* , since it is precisely twice of f_y^* . It seems that the lock-in phenomena are caused near the tip of the cylinder ($z/L=0.9$), since the frequency of vortex shedding is almost equal to that of oscillation as shown in Fig. 11. However, similar phenomena are not seen in the mid-span of the cylinder ($z/L=0.5$). It is thought that these phenomena depend upon the type of the spanwise amplitude distribution.

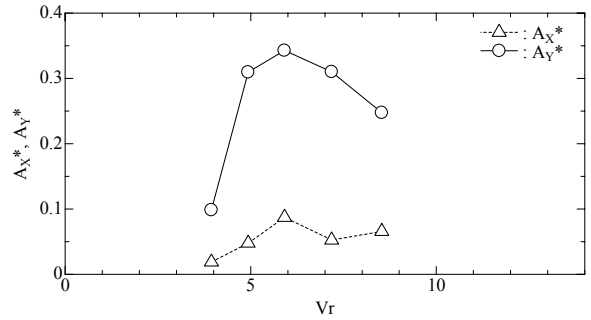


Figure 10: Amplitude response of the cylinder tip for the reduced velocity.

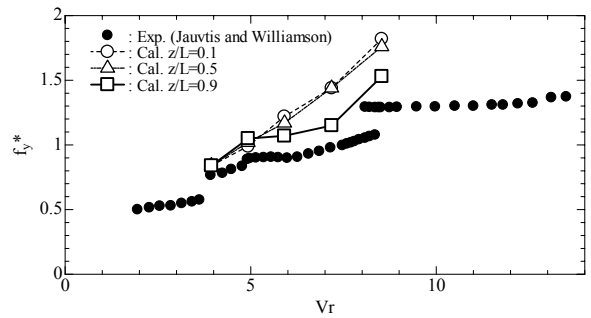


Figure 11: Frequency Response of lift force for the reduced velocity.

4. CONCLUSION

A fully coupled methodology is developed for calculation of the flow-structure interaction problems with moving and deforming mesh systems. And a virtual wind tunnel using a vortex element method has been constructed.

In order to confirm the applicability of our code, flow simulation around a stationary circular

cylinder and flexible cantilever circular cylinder were performed. The response amplitudes obtained by present calculations were similar to the experimental results, though these amplitudes obtained by present calculations were somewhat smaller than the experimental results. It was confirmed that the lock-in phenomena are caused near the tip of the cylinder

From the results of the present study, it is concluded that the virtual wind tunnel based on the vortex method, is available and useful for research of flow induced vibrations.

5. REFERENCES

- Dhondt, G., *CalculiX USER'S MANUAL* version 1.5, (1998-2004).
- Evangelinos, C., Lucor, D. and Karniadakis, G.E., 2000, DNS-derived force distribution on flexible cylinders subject to vortex-induced vibration, *J. Fluids and Structures* 14 (3): 429-440.
- Feng, C.C., 1968, The measurement of vortex-induced effects in the flow past stationary and oscillating circular and D-section cylinders, MS thesis, University of British Columbia.
- Flemming, F. and Williamson, C.H.K., 2005, Vortex-induced vibrations of a pivoted cylinder, *J. Fluid Mech.*, Vol.552: 215-252.
- Fukuda K., and Kamemoto, K., 2005, Application of a redistribution model incorporated in a vortex method to turbulent flow analysis, *ICVFM2005*, Yokohama, Japan: 131-136.
- Greengard, L. and Rohklin, V., 1987, A fast algorithm for particle simulations, *J. Comp. Phys.* 73: 325-348.
- Jauvtis, N. and Williamson, C.H.K., 2004, The effect of two degrees of freedom on vortex-induced vibration at low mass and damping, *J. Fluid Mech.*, Vol.509: 23-62.
- Kamemoto, K., 1995, On attractive features of the vortex methods, *Computational Fluid Dynamics Review*, ed. M.Hafez and K.Oshima, JOHN WILEY & SONS: 334-353.
- King, R., 1977, A review of vortex-shedding research and its application, *Ocean Eng.* 4: 141-171.
- Leonard, A., 1980, Vortex methods for flow simulations, *J. Comp. Phys.* 37: 289-335.
- Meneghini, J.R. and Bearman, P.W., 1995, Numerical simulation of high amplitude oscillatory flow about a circular cylinder, *J. Fluids and Structures* 9 (4): 435-455.
- Nakanishi, Y. and Kamemoto, K., 1992, Numerical simulation of flow around a sphere with vortex blobs, *Journal Wind Eng. and Ind. Aero*, Vol. 46 & 47: 63-369.
- Ojima A. and Kamemoto, K., 2000, Numerical simulation of unsteady flows around three-dimensional bluff bodies by an advanced vortex method, *JSME Int. Journal*, 43-2 B: 127-135.
- Sarpkaya, T., 1989, Computational methods with vortices - the 1988 Freeman scholar lecture, *J. Fluids Engng.*, 111: 5-52.
- Uhlman, J.S., 1992, An integral equation formulation of the equation of motion of an incompressible fluid, *Naval Undersea Warfare Center T.R.*, 10 086.
- Willden, R.H.J. and Graham, J.M.R., 2001, Numerical prediction of VIV on long flexible circular cylinders, *J. Fluids and Structures* 15 (3-4): 659-669.
- Williamson, C.H.K., 1989, Oblique and parallel modes of vortex shedding in the wake of a circular cylinder at low Reynolds numbers, *J. Fluid Mech.*, Vol.206: 579-627.
- Winkelmann, G. and Leonard, A., 1988, Improved vortex methods for three-dimensional flows, *Proc. Workshop on Mathematical Aspects of Vortex Dynamics*, pp.25-35, Leeburg, Virginia.
- Wu, J.C. and Thompson, J.F., 1973, Numerical solutions of time-dependent incompressible Navier-Stokes equations using an integro-differential formulation, *Computers & Fluids*, Vol. 1: 197-215.
- Zhou, C.Y., So, R.M., and Lam, K., 1999, Vortex-induced vibrations of an elastic circular cylinder, *J. Fluids and Structures* 13 (2): 165-189.